Self-surfactant effect in graphene growth on Pt(111)

Xingxing Dong,[1] Changchun He,[1] Chao He,[1] Xiaowei Liang,[1] Shaogang Xu,[1] and Hu Xu[1,2,3,*]

[1]*Department of Physics, Southern University of Science and Technology, Shenzhen 518055, People's Republic of China*

[2]*Quantum Science Center of Guangdong–Hong Kong–Macao Greater Bay Area (Guangdong), Shenzhen 518045, People's Republic of China*

[3]*Shenzhen Key Laboratory for Advanced Quantum Functional Materials and Devices, Southern University of Science and Technology, Shenzhen 518055, People's Republic of China*

(Received 29 March 2023; revised 3 July 2023; accepted 8 September 2023; published 19 September 2023)

Graphene, a material with exceptional physicochemical properties, has been synthesized on a variety of substrates. However, prior theoretical studies have suggested that carbon (C) clusters are typically less stable thermodynamically compared to individual C monomers on most transition metal substrates. Taking the Pt(111) surface as a case study, we introduce a unified mechanism termed the "self-surfactant effect" that promotes the efficient growth of graphene on Pt(111). This mechanism incorporates two key processes: edge passivation and repulsion minimization. The self-surfactant effect serves as an essential bridge between theoretical predictions and experimental observations, enhancing the growth of graphene in two ways: (1) by strengthening the interaction between C clusters and the substrate through edge passivation, and (2) by minimizing repulsion between the inner atoms of C clusters and the substrate. Intriguingly, our results reveal a linear correlation between the formation energies of C clusters on the Pt(111) surface and the ratio of peripheral atoms to the total number of atoms within the clusters. These insights not only advance our understanding of graphene growth but may also have broader implications for other heteroepitaxial systems.

DOI: 10.1103/PhysRevB.108.125425

I. INTRODUCTION

Graphene, a monolayer of sp^2-hybridized carbon atoms, possesses unique properties and extensive potential applications, attracting significant interest across various research fields [1–3]. To fully exploit its potential, the development of reliable methods for synthesizing large-area, high-quality graphene is crucial. Although the exfoliation of graphene from bulk graphite has been actively explored [4–6], obtaining samples suitable for practical device applications remains challenging. Epitaxial growth on suitable substrates has emerged as a promising approach to produce large, uniform graphene samples in a cost-effective manner. Various transition metal substrates, including Cu [7], Ni [8], Ru [9], Rh [10], Ir [11], and Pt [12–15], have been utilized for graphene synthesis.

While atomic-scale growth mechanisms on certain substrates have been identified [16,17], these mechanisms do not universally apply to all metal substrates. Earlier theoretical calculations have suggested that graphene nucleation on Rh(111), Ir(111), Pt(111), and Pd(111) is highly unlikely, given that C dimers show significantly higher formation energies than C monomers [18]. Furthermore, C_{10} clusters on Ir(111) [19] and C_{24} clusters on Rh(111) [20] are energetically less favorable than C monomers. Thus, the experimentally observed formation of graphene cannot be accounted for merely by the aggregation of C atoms into clusters, considering the high stability of C monomers should deter such aggregation. As the consistent incorporation of C atoms allows C clusters to expand into larger graphene islands, exploring the interaction and stable configuration of C clusters during nucleation and growth may help resolve this discrepancy. The Pt(111) substrate is particularly interesting due to its superior catalytic activity and minimal effect on the properties of graphene [12,13]. Additionally, various moiré patterns can emerge during graphene growth on Pt(111) due to the weak graphene-substrate interaction [12–14]. Previous work [21] has proposed that this weak interaction induces separated vacancies on the substrate surface, resulting in a $\sqrt{3} \times \sqrt{3}$ phase of graphene. Interestingly, surface vacancies induced by atom deposition may suggest a self-surfactant effect in epitaxial growth [22,23], as observed in the growth of silicene and borophene on Ag(111) [24,25]. Therefore, an in-depth analysis of the interactions between C clusters and the Pt(111) substrate is essential for elucidating the underlying growth mechanism of graphene.

In this work, we employ density functional theory (DFT) to examine the energetics and dynamics of graphene growth on Pt(111). Contrary to traditional aggregation theories, our analysis reveals a unique self-surfactant effect that optimizes interactions by passivating the peripheral atoms of C clusters. This effect is substantiated by a linear correlation between the formation energies of C clusters and the ratio of peripheral to total atoms (N_P/N_T). Importantly, this self-surfactant effect offers a compelling explanation for experimental observations, including morphological changes at step edges and the preferential formation of larger graphene islands near steps.

*xuh@sustech.edu.cn

II. COMPUTATIONAL DETAILS

We employ DFT as implemented in the Vienna *Ab initio* Simulation Package (VASP) for all calculations [26,27]. The generalized gradient approximation with the Perdew-Burke-Ernzerhof formalism is used to describe the exchange correlation energy [28]. The van der Waals correction (DFT-D3) is employed to treat the interlayer interactions between C clusters and the Pt(111) surface [29]. The energy cutoff for plane-wave expansion is set at 450 eV, and the force convergence criterion is 0.02 eV/Å. Our models consist of a four-layer Pt slab. The lattice constants employed are 2.81 Å for Pt and 2.46 Å for graphene, which are consistent with the previous works [30–33]. Gamma-centered k-point sampling is used, with a $3 \times 3 \times 1$ grid for the 4×4 supercell and a $2 \times 2 \times 1$ grid for the 6×6, 7×7, and 9×9 supercells. A vacuum layer of 12 Å is introduced to prevent interactions between adjacent images. During geometric optimization, the bottom two layers of the Pt(111) substrate are kept fixed to mimic the bulk environment. The energy barriers are determined using the climbing image nudged elastic band (CI-NEB) method [34].

The formation energy (E_f) of C clusters per C atom on Pt(111) is defined by the following equation:

$$E_f = \frac{E_{\text{total}} - E_{\text{sub}} - N_{\text{C}} \times \mu_C - N_{\text{Pt}} \times \mu_{\text{Pt}}}{N_{\text{C}}},$$

where E_{total} and E_{sub} denote the total energy of the system and the energy of the Pt substrate, respectively. μ_{C} and μ_{Pt} are chemical potentials of C and Pt in their most stable bulk phases, namely graphite and face-centered cubic platinum, respectively. N_{Pt} and N_{C} refer to the number of Pt atoms involved in evaluating the structural stability of C clusters and the number of C atoms, respectively.

III. RESULTS AND DISCUSSION

A. Growth on the terrace

We begin by examining small C clusters C_N ($N = 1 \sim 10$) on the Pt(111) surface. Traditional growth mechanisms suggest that these C clusters rest on the substrate with their edges bonded to surface metal atoms [35], a process we refer to as aggregation on the terrace (A-OT). For a C monomer, we consider five typical adsorption sites on Pt(111): top, fcc hollow (fcc), hcp hollow (hcp), subsurface tetrahedral (tetr), and subsurface octahedral (oct) sites, as depicted in Fig. 1(a). The corresponding E_f values are 2.83, 0.50, 0.73, 0.72, and 1.27 eV, respectively, indicating that the preferred site for C monomer to be fcc [36]. We find that the E_f of a C monomer at the subsurface tetrahedral and octahedral sites are 0.22 eV and 0.77 eV higher, respectively, than that for the fcc hollow site. This is in agreement with previous findings indicating low carbon solubility in Pt [37]. We also conduct a comprehensive analysis of various C_N ($N = 2, \ldots, 10$) structures, including one-dimensional (1D) chains and 2D networks (see Figs. S1 and S2 of the Supplemental Material [38]). Consistent with other transition metal substrates, 1D chain structures exhibit greater stability than their 2D counterparts during the initial stages of graphene growth on Pt(111) [19,35]. The relative stability of these C clusters is summarized in Fig. 2, with the dashed line representing the most stable fcc hollow site for a C monomer. Remarkably, the C monomer is more stable than all other clusters in the A-OT growth mode, indicating that C monomers are unlikely to aggregate into larger clusters on the Pt(111) terrace. However, the E_f of graphene on Pt(111) is approximately −0.103 eV/atom [33,39], significantly lower than that of a C monomer on Pt(111), as confirmed by previous calculations [33,39]. This discrepancy challenges the A-OT mechanism, suggesting the need for an alternative mechanism for graphene growth on Pt(111).

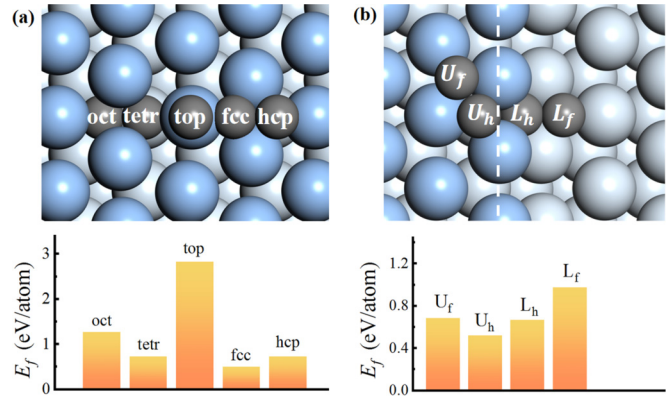

FIG. 1. Top views of adsorption sites and E_f of a C monomer (a) on the terrace and (b) near the step of Pt(111). Light blue, gray white, and umbra gray spheres represent Pt atoms on the upper terrace, Pt atoms on the lower terrace, and C atoms, respectively. The white dashed line indicates the step edge.

To understand why C clusters are unstable on Pt(111), we carefully examine the interactions between C clusters and the substrate. The E_f of a C cluster on the Pt(111) surface consists of two components: the binding energy among C atoms within the cluster ($E_{\text{C–C}}$) and the adsorption energy

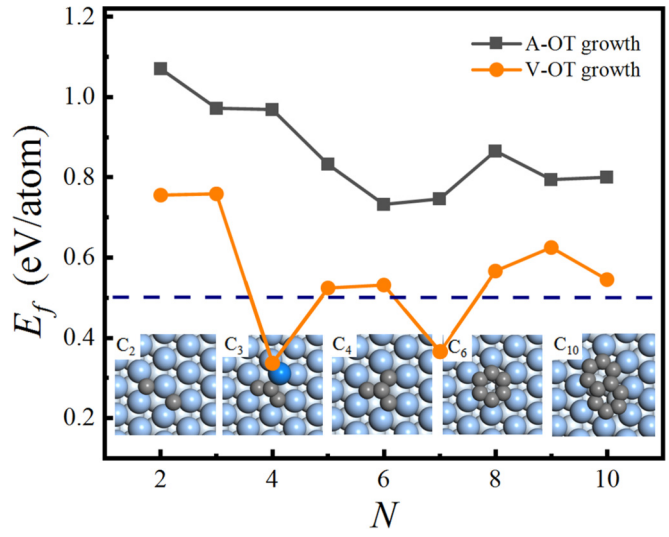

FIG. 2. The relative stability of C clusters as a function of C atoms based on A-OT and V-OT mechanisms on the terrace. Insets depict representative structures of C_N based on the V-OT mechanism. The blue sphere represents the expelled Pt atom, while the dotted line signifies the C monomer at the most favorable fcc site.

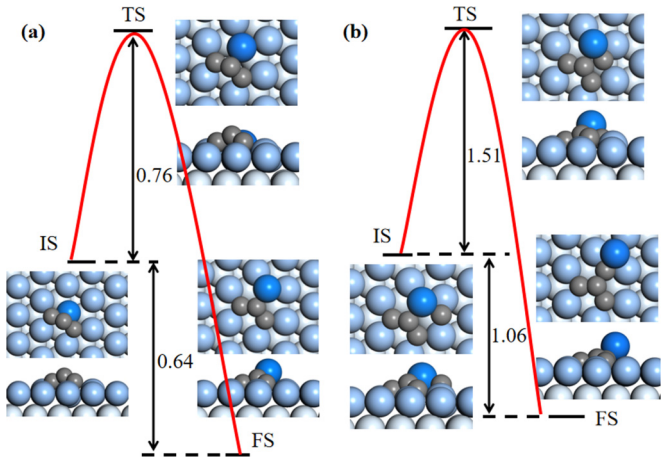

FIG. 3. Reaction pathways and barriers (in units of eV) for forming one Pt vacancy with (a) three and (b) four C atoms on the terrace.

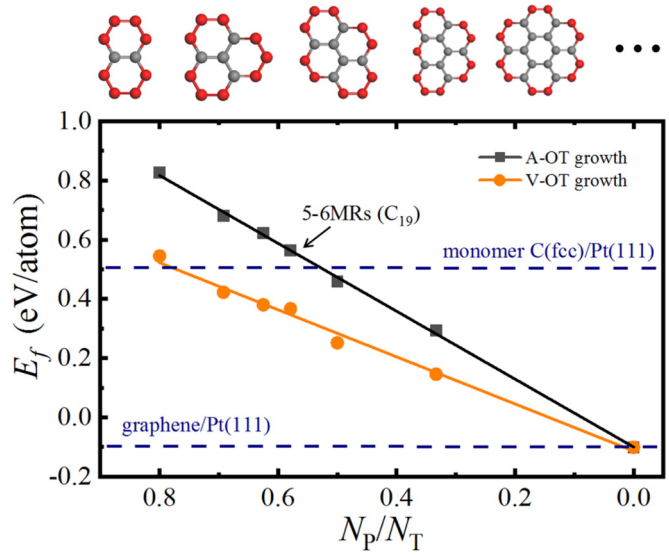

FIG. 4. E_f of X-6MR clusters on Pt(111) as a function of N_P/N_T (X = 2, 3, 4, 5, 7, and 19). The peripheral C atoms are highlighted in red.

of the cluster on the Pt(111) surface (E_{C-Pt}). Interestingly, these two components exhibit opposite trends as the size of the C cluster increases [40]. While E_{C-C} decreases, it fails to counterbalance the increase in E_{C-Pt}, resulting in higher E_f values for larger C clusters compared to a C monomer. Therefore, minimizing E_{C-Pt} is essential for enhancing the stability of C clusters on Pt(111). Upon structural relaxation, we observe that the edges of C clusters bend toward the terrace, forming arched chains or 2D structures. This suggests strong interactions between the cluster edges and the substrate. Additionally, graphene islands exhibit stronger binding at step edges compared to terraces, attributed to the increased reactivity of step atoms. Based on these findings, we propose that C clusters induce Pt vacancies during graphene growth on Pt(111), allowing their edges to be terminated by more reactive metal atoms.

We investigate small C clusters formed by inducing a vacancy on the terrace (V-OT), with their E_f and some typical structures shown in Fig. 2. In agreement with prior calculations [18], a stable configuration for two C atoms is achieved when each C atom occupies a separate fcc site. This results in an E_f that is 0.31 eV/atom lower than a dimer formed by one C atom on an fcc site and another at an adjacent hcp site. Figure 2 presents a scenario where a Pt atom is removed by three C atoms (i.e., C_3), creating a Pt vacancy. In the C_3 cluster, the two peripheral C atoms occupy fcc hollow sites terminated by highly active metal atoms, while the inner C atom bonds with the expelled Pt atom. This offsets the energy used by the ejected Pt atom, yielding a significantly lower E_f value (by 0.64 eV) compared to an arched C_3 chain situated on the ideal terrace.

To validate the reliability of the V-OT mechanism, we investigate the formation process of the Pt vacancy, as shown in Fig. 3(a). The energy barrier for creating a single Pt vacancy on the terrace is 0.76 eV, which is easily overcome at the high experimental growth temperatures of around 1000 °C [13,41]. As depicted in Fig. 3(b), the addition of a fourth C atom replaces the previously ejected Pt atom, releasing an energy of 1.06 eV. This energy release facilitates the diffusion of the expelled Pt atom, resulting in a Pt vacancy on the terrace. The C_4 cluster preferentially occupies this vacancy, forming the smallest planar C_4 structure with peripheral C atoms terminated by reactive metal atoms. The inner and peripheral C atoms form sp^2 and sp^2-like bonds (one C-C bond and two C-Pt bonds), respectively. The C_5 and C_6 clusters have five- and six-membered ring configurations at the vacancy site. As the size of C clusters increases, additional Pt atoms are removed to optimize edge termination, as shown in Fig. S3 [38]. To summarize briefly, small C clusters formed via the V-OT mechanism exhibit greater stability compared to those formed through the A-OT mechanism, suggesting its potential advantages for graphene growth process on Pt(111). We extend our investigation to larger C clusters (C_N, where $N > 10$) on the Pt(111) terrace, focusing exclusively on 2D structures composed of 6-membered rings (6MRs). This is in line with previous findings that larger C clusters favor 2D networks over 1D chains on transition metal surfaces [17]. We evaluate these structures, denoted as X-6MRs (where X represents the number of 6MRs), under both the A-OT and V-OT growth mechanisms. The E_f of X-6MRs as a function of the ratio of N_P/N_T is presented in Fig. 4. Two dashed lines represent the limiting cases of a C monomer and graphene. Remarkably, the V-OT mechanism emerges as energetically favorable for C cluster growth, with the energy difference between the two mechanisms decreasing as the proportion of peripheral atoms diminishes. Interestingly, a linear correlation exists between E_f and N_P/N_T, which can be fitted by the following equations:

$$E_f^{\mathrm{AOT}}(\mathrm{terrace}) = 1.147 \times \frac{N_P}{N_T} - 0.100\ \mathrm{eV}, \quad (1)$$

$$E_f^{\mathrm{VOT}}(\mathrm{terrace}) = 0.795 \times \frac{N_P}{N_T} - 0.103\ \mathrm{eV}. \quad (2)$$

Here, the coefficients represent the energy difference between peripheral and inner C atoms ($E_f^P - E_f^I$), while the constants correspond to the E_f contributed by an inner C atom (E_f^I). A detailed derivation is available in Sec. A of the Supplemental

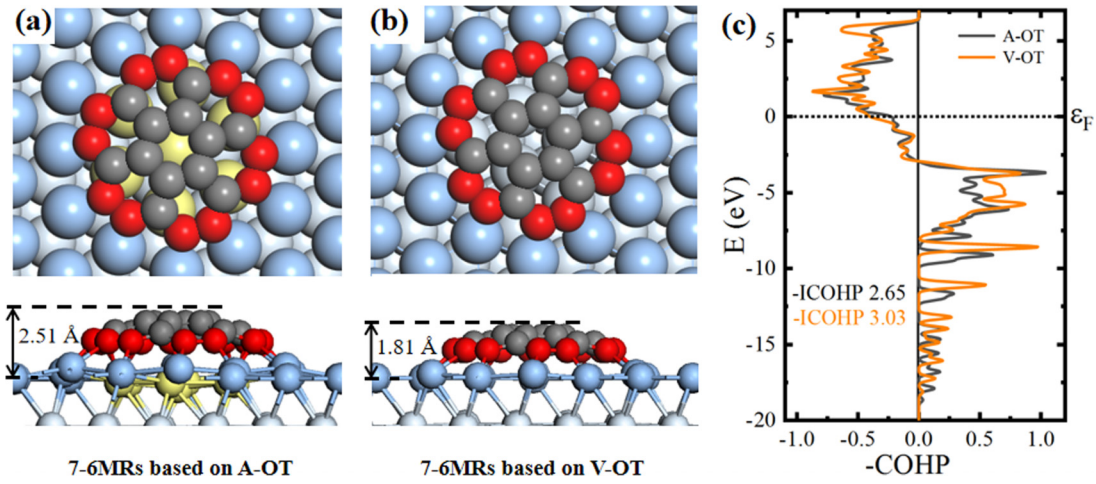

FIG. 5. Top and side views of 7-6MRs based on (a) A-OT and (b) V-OT mechanisms. The Pt atoms directly below the cluster are shown in light yellow. (c) −COHP analysis for 7-6MRs formed by A-OT (black line) and V-OT (orange line) mechanisms.

Material [38]. For both mechanisms, the E_f^I is approximately −0.103 eV/atom, attributable to the saturation of inner C atoms by sp^2 C-C bonds, similar to graphene. Transitioning from A-OT to V-OT results in a significant eduction in E_f^P from 1.047 eV to 0.692 eV, which we attribute to the termination of C clusters by more reactive metal atoms. To deepen our understanding of the interactions between peripheral C atoms and the substrate, we employ the crystal orbital Hamilton population (COHP) method [42]. Figure 5(c) shows the COHP analysis for the 7-6MR cluster formed via both mechanisms. Positive COHP values indicate bonding contributions, while negative values signify antibonding contributions. A noticeable difference in bonding strength is observed between the two mechanisms, particularly around −5 eV. We quantify the C-Pt bond strength using the integrated COHP (ICOHP) values, which are 2.65 and 3.03 for the A-OT and V-OT mechanisms, respectively. A higher ICOHP value implies stronger bonding, corroborating the preference for the V-OT mechanism in enhancing C cluster edge bonding with substrates.

Another noteworthy aspect of Pt vacancies is their role in mitigating the electrostatic repulsion between C clusters and the substrate. This is evidenced by the noticeable downward shift of Pt atoms situated directly beneath the C clusters. For instance, in the A-OT mechanism depicted in Fig. 5(a), seven surface Pt atoms beneath the 7-6MRs (highlighted in yellow) undergo a downward shift of approximately 0.35 Å to attain equilibrium. This configuration represents the most stable state, as determined through extensive analysis of the 7-6MRs' rotational and translational movements on the terrace (see Sec. C of the Supplemental Material [38]). We also explore origins of the electrostatic repulsion between the inner region of the C cluster and the substrate. Figure 5(a) reveals that the strong interaction between the peripheral C atoms and the substrate results in an archlike dome of 7-6MRs, standing at a height of 2.51 Å and an average C-Pt bond length of 2.06 Å. The distance between the inner C atoms and the substrate (about 2.86 Å) is less than the equilibrium separation of 3.44 Å between graphene and the Pt surface [13,33]. This suggests that the inner C atoms experience electrostatic repulsion with the surface Pt atoms, causing the latter to shift downward. An equilibrium is eventually reached, counterbalanced by the repulsion between these descending atoms and the subsurface atoms. The removal of surface Pt atoms significantly reduces this repulsion, thereby enhancing C cluster stability, as illustrated in Fig. 5(b). This is further supported by a reduced arch height of 1.81 Å and a shorter average C-Pt bond length of 1.99 Å. In this case, the E_f is 0.25 eV/atom, significantly lower than that of 7-6MRs on an ideal terrace. Furthermore, we examine the influence of subsurface Pt vacancies, as shown in Fig. S5 [38]. Our findings indicate that these subsurface vacancies do not offer an energy benefit compared to surface Pt vacancies. This is primarily due to the significant increase in substrate energy caused by subsurface vacancy defects. The resulting reduction in electrostatic interaction between the C clusters and the subsurface of the substrate is insufficient to offset this energy increase. Consequently, we conclude that both peripheral atom passivation and vacancy formation play significant roles in strengthening the bonding between peripheral atoms and the substrate, while simultaneously reducing repulsive interactions with the inner atoms. This self-surfactant effect ultimately facilitates the growth of graphene on the Pt(111) terrace.

B. Growth near the step

Considering the presence of various surface steps in real experiments, it is essential to study the growth of graphene near the steps on the Pt(111) surface. For a C monomer, four hollow adsorption sites near the step on the Pt(111) surface are considered: U_f, U_h, L_h, and L_f. These sites correspond to the (U) upper surface of a step, (L) lower surface of a step, (h) hcp site, and (f) fcc site, respectively. Among these sites, the U_h site is the most favorable adsorption site ($E_f = 0.52$ eV/atom), which is 0.14 eV/atom lower in energy than that of the L_h site. As a result, in contrast to previous investigations that solely focus on clusters supported by the lower surface of a step [17], the upper surface also emerges as a viable nucleation candidate. On the lower surface, small C

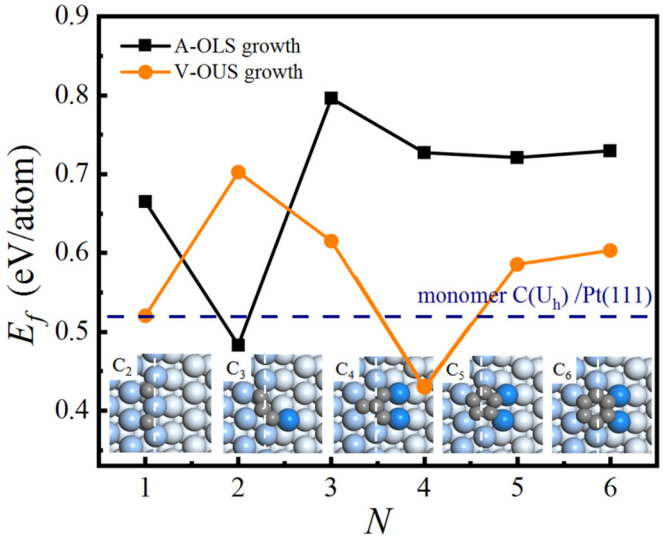

FIG. 6. E_f of C_N based on A-OLS and V-OUS mechanisms near a step on Pt(111). The structures of C clusters supported on the upper surface are shown in the insets.

clusters can attach to the step to form chains or ringlike structures. Ringlike structures are more stable because C chains parallel to the step are not well accommodated [19] (see Sec. D of the Supplemental Material [38]). The E_f of these clusters are shown in Fig. 6. For the aggregation growth mechanism on the lower surface of a step (A-OLS), the C dimer is more stable than all other clusters, indicating that C atoms cannot aggregate into clusters larger than C_2 near the step. In other words, A-OLS also faces the instability problem of C clusters.

Based on the above discussion, we introduce a unified growth mechanism on the upper surface of a step (V-OUS) that addresses the instability issue by terminating the peripheral atoms of C clusters with highly reactive metal atoms. Representative clusters following the V-OUS mechanism are illustrated in the insets of Fig. 6. For a C dimer, each atom occupies the energetically favorable U_h site. The ground state of C_3 forms a chain that displaces one Pt atom from the step, while the most stable C_4 configuration is a three-pronged structure with one inner atom and three peripheral atoms. As with the terrace case, C_5 and C_6 adopt five- and six-membered ring configurations, respectively. Except for C_2, where the dimer on the lower surface is more stable, small clusters on the upper surface of a step are energetically preferred.

To validate the V-OUS mechanism, we examine the growth kinetics, as depicted in Fig. 7. The energy barrier for creating a Pt vacancy at the step, induced by a C_3 chain, is 0.65 eV, which is lower than 0.76 eV barrier on a terrace. This suggests a faster growth rate near steps, corroborating experimental observations of larger graphene islands near steps [14]. The formation of C_4 involves the sequential addition of a C atom and a Pt atom, as shown in Figs. 7(b) and 7(c). The incorporation of an additional C atom requires overcoming an energy barrier of 0.71 eV, while reducing the total energy by 0.28 eV. The subsequent addition of a Pt adatom is highly exothermic, releasing 2.27 eV of energy with a minimal energy barrier of 0.14 eV.

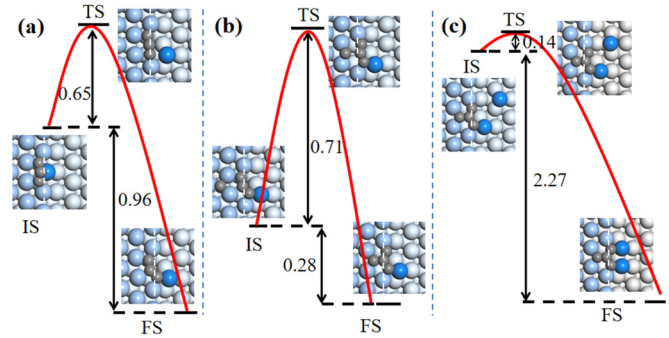

FIG. 7. (a) The process of a Pt vacancy induced by a C_3 chain. (b) The process of incorporating a C atom onto a C_3 chain. (c) The process of adding a Pt atom to form the most stable C_4 structure. Energy barriers are in units of eV.

Our analysis, summarized in Fig. 8, reveals that C cluster stability increases with size. The E_f of X-6MR clusters also exhibits a linear correlation with N_P/N_T, well fitted by the equation

$$E_f^V(\text{step}) = 0.728 \times \frac{N_P}{N_T} - 0.106\ \text{eV}, \tag{3}$$

where the coefficient and constant term represent $(E_f^P - E_f^I)$ and E_f^I, respectively. Notably, E_f^I is approximately -0.103 eV, indicating that, similar to the terrace case, only the peripheral atoms of X-6MRs bond to the substrate. However, E_f^P is 0.07 eV lower than on the terrace, attributable to the lower coordination number of metal atoms terminating the edges of C_N clusters, as represented by the blue atoms in Fig. 8. These more reactive atoms enhance the interaction between C clusters and the substrate, reinforcing the role of steps in facilitating graphene growth. This aligns well with experimental observations of significant mass transport on Pt steps [14].

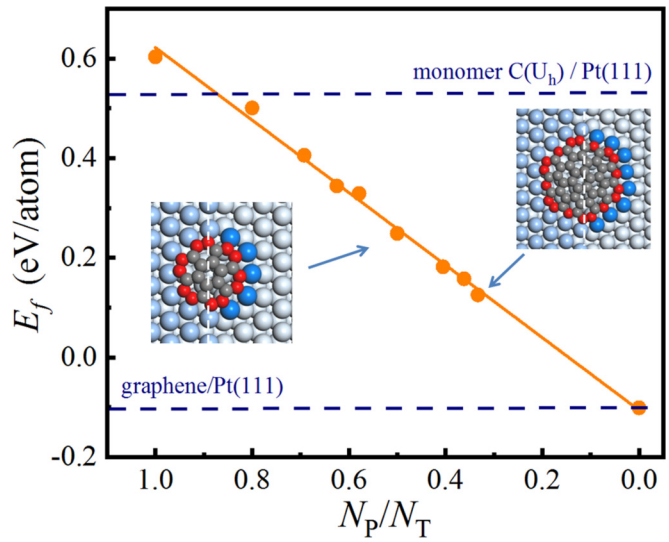

FIG. 8. E_f of X-6MR clusters near the step as a function of N_P/N_T (X = 1, 2, 3, 4, 5, 7, 12, 16, and 19).

C. Comparison with experimental results

Previous theoretical studies have shown that C clusters exhibit higher formation energies than C monomers when interacting with various transition metal substrates [18–20]. This observation raises questions about the conventional understanding of graphene formation through the aggregation of C atoms into clusters [10–15]. In our study focusing on the Pt(111) surface, we find that the stability of C clusters hinges on two key interactions: the attractive forces between the peripheral atoms of the clusters and the substrate, and the repulsive forces experienced by the inner atoms of the clusters with respect to the substrate. A balanced interplay between these forces is crucial for the stability and subsequent growth of graphene clusters. Through our detailed calculations, we identify that the self-surfactant effect can meet both of these criteria, thereby offering a plausible mechanism for graphene growth. Specifically, we find that the attractive interactions between the peripheral atoms of C clusters and the substrate are significantly enhanced when these peripheral atoms are passivated by more reactive, step-edge atoms rather than surface atoms. Simultaneously, the repulsive interactions between the inner atoms and the substrate are mitigated by increasing their separation distance. This understanding aligns well with experimental observations and provides a more comprehensive framework for interpreting the growth of graphene on transition metal substrates.

Crucially, a range of experimental evidence lends further support to the role of the self-surfactant effect in facilitating graphene growth on Pt(111). First, the adsorption energy of a C monomer at subsurface sites is consistently found to be higher than at surface fcc hollow sites. This suggests low carbon solubility in the Pt substrate, reinforcing the idea that graphene growth on Pt(111) is largely driven by a surface-mediated process [37]. Second, it has been observed that graphene islands preferentially nucleate at the upper regions of steps, and these step edges are not perfectly linear [14,15,43]. These findings are in agreement with our calculations, which identify the upper surface as the most energetically favorable site for adsorption. In addition, the self-surfactant effect is shown to induce significant mass transfer along the substrate. Third, larger graphene islands have been observed to form near steps as opposed to terraces [14,15]. This is consistent with our results, which indicate a lower energy barrier for Pt vacancy formation when induced by a C_3 chain at the step edge, suggesting a faster growth rate near steps. Bright lines surrounding graphene islands, as observed experimentally, align well with our hypothesis that the edges of these clusters are terminated by more reactive metal atoms. This is a direct manifestation of the self-surfactant effect [14].

Our decision to exclude the effects of hydrogen from our calculations is a deliberate and justified simplification, particularly given the frequent use of hydrocarbons as C sources in graphene synthesis. During the early stages of graphene growth, hydrocarbons undergo catalytic decomposition on metal surfaces, producing reactive C species. For instance, previous experimental work [44] has shown that temperatures exceeding 430 K lead to the complete desorption of hydrogen atoms from ethylene adsorbed on Pt(111), leaving only C atoms on the surface. Given that the experimental growth of graphene commonly occurs at significantly higher temperatures, often around 1000 °C [13,41], the influence of hydrogen in this process can be considered negligible. Furthermore, we note that hydrogen-free graphene growth has been widely reported on various substrates, such as metals and hexagonal boron nitride (h-BN), using methods such as molecular beam epitaxy [45–48]. These findings lend further support to our approach, further supporting the viewpoint that such an exclusion is a reasonable simplification, allowing us to focus more closely on specific aspects of the graphene growth process.

IV. CONCLUSIONS

In conclusion, we have investigated the growth mechanisms of graphene on Pt(111). Our findings indicate that the conventional wisdom of C monomers aggregating into clusters on a pristine Pt(111) surface is challenged by the weakening interaction between increasing C cluster sizes and the substrate. To address this issue, we introduce the concept of a self-surfactant effect, which serves to strengthen the bonding between the peripheral atoms of C clusters and highly reactive metal atoms, while simultaneously reducing the repulsive forces experienced by the inner atoms of the clusters.

Significantly, we uncovered a robust linear relationship between E_f of C clusters and the ratio of peripheral to total atoms (N_P/N_T). This relationship quantitatively emphasizes the importance of the chemical environment of peripheral atoms in determining cluster stability. Importantly, our theoretical insights align well with experimental data, particularly the preferential formation of graphene islands at the upper steps of Pt(111) surfaces. The observed larger sizes of these islands near steps, as compared to those on terraces, can be attributed to a reduced energy barrier for Pt vacancy formation at these locations. Considering that C monomers also exhibit greater stability on a variety of other ideal transition metal substrates, we anticipate that the self-surfactant effect in graphene growth could potentially extend to a broader range of substrates. Overall, our studies highlight the crucial role of sample-substrate interactions in understanding the epitaxial growth of materials, offering valuable insights for the rational design of promising materials with tailored properties.

ACKNOWLEDGMENTS

This work is supported by the National Natural Science Foundation of China (Grants No. 12374182 and No. 11974160), the Science, Technology, and Innovation Commission of Shenzhen Municipality (Grant No. RCYX20200714114523069), and the Center for Computational Science and Engineering at Southern University of Science and Technology.

[1] A. K. Geim, Graphene: Status and prospects, Science **324**, 1530 (2009).

[2] M. D. Stoller, S. Park, Y. Zhu, J. An, and R. S. Ruoff, Graphene-based ultracapacitors, Nano Lett. **8**, 3498 (2008).

[3] K. S. Novoselov, V. I. Fal'ko, L. Colombo, P. R. Gellert, M. G. Schwab, and K. Kim, A roadmap for graphene, Nature (London) **490**, 192 (2012).

[4] K. S. Novoselov, A. K. Geim, S. V. Morozov, D. Jiang, M. I. Katsnelson, I. Grigorieva, S. Dubonos, and A. Firsov, Two-dimensional gas of massless Dirac fermions in graphene, Nature (London) **438**, 197 (2005).

[5] M. Yi and Z. Shen, A review on mechanical exfoliation for the scalable production of graphene, J. Mater. Chem. A **3**, 11700 (2015).

[6] Y. Hernandez, V. Nicolosi, M. Lotya, F. M. Blighe, Z. Sun, S. De, I. T. McGovern, B. Holland, M. Byrne, Y. K. Gun'Ko *et al.*, High-yield production of graphene by liquid-phase exfoliation of graphite, Nat. Nanotechnol. **3**, 563 (2008).

[7] L. Gao, J. R. Guest, and N. P. Guisinger, Epitaxial graphene on Cu(111), Nano Lett. **10**, 3512 (2010).

[8] Y. S. Dedkov, M. Fonin, U. Rüdiger, and C. Laubschat, Rashba Effect in the Graphene/Ni(111) System, Phys. Rev. Lett. **100**, 107602 (2008).

[9] P. W. Sutter, J.-I. Flege, and E. A. Sutter, Epitaxial graphene on ruthenium, Nat. Mater. **7**, 406 (2008).

[10] M. Sicot, P. Leicht, A. Zusan, S. Bouvron, O. Zander, M. Weser, Y. S. Dedkov, K. Horn, and M. Fonin, Size-selected epitaxial nanoislands underneath graphene moiré on Rh(111), ACS Nano **6**, 151 (2012).

[11] J. Coraux, T. N. Plasa, C. Busse, T. Michely *et al.*, Structure of epitaxial graphene on Ir(111), New J. Phys. **10**, 043033 (2008).

[12] M. Gao, Y. Pan, L. Huang, H. Hu, L. Zhang, H. Guo, S. Du, and H.-J. Gao, Epitaxial growth and structural property of graphene on Pt(111), Appl. Phys. Lett. **98**, 033101 (2011).

[13] P. Sutter, J. T. Sadowski, and E. Sutter, Graphene on Pt(111): Growth and substrate interaction, Phys. Rev. B **80**, 245411 (2009).

[14] T. Land, T. Michely, R. Behm, J. Hemminger, and G. Comsa, STM investigation of single layer graphite structures produced on Pt(111) by hydrocarbon decomposition, Surf. Sci. **264**, 261 (1992).

[15] T. Fujita, W. Kobayashi, and C. Oshima, Novel structures of carbon layers on a Pt(111) surface, Surf. Interface Anal. **37**, 120 (2005).

[16] Y. Li, M. Li, T. Wang, F. Bai, and Y.-X. Yu, DFT study on the atomic-scale nucleation path of graphene growth on the Cu(111) surface, Phys. Chem. Chem. Phys. **16**, 5213 (2014).

[17] J. Gao, J. Yip, J. Zhao, B. I. Yakobson, and F. Ding, Graphene nucleation on transition metal surface: Structure transformation and role of the metal step edge, J. Am. Chem. Soc. **133**, 5009 (2011).

[18] H. Chen, W. Zhu, and Z. Zhang, Contrasting Behavior of Carbon Nucleation in the Initial Stages of Graphene Epitaxial Growth on Stepped Metal Surfaces, Phys. Rev. Lett. **104**, 186101 (2010).

[19] P. Wu, H. Jiang, W. Zhang, Z. Li, Z. Hou, and J. Yang, Lattice mismatch induced nonlinear growth of graphene, J. Am. Chem. Soc. **134**, 6045 (2012).

[20] B. Wang, X. Ma, M. Caffio, R. Schaub, and W.-X. Li, Size-selective carbon nanoclusters as precursors to the growth of epitaxial graphene, Nano Lett. **11**, 424 (2011).

[21] G. Otero, C. González, A. L. Pinardi, P. Merino, S. Gardonio, S. Lizzit, M. Blanco-Rey, K. Van de Ruit, C. F. J. Flipse, J. Méndez, P. L. de Andrés, and J. A. Martín-Gago, Ordered Vacancy Network Induced by the Growth of Epitaxial Graphene on Pt(111), Phys. Rev. Lett. **105**, 216102 (2010).

[22] B.-G. Liu, J. Wu, E. G. Wang, and Z. Zhang, Two-Dimensional Pattern Formation in Surfactant-Mediated Epitaxial Growth, Phys. Rev. Lett. **83**, 1195 (1999).

[23] Z. Zhang and M. G. Lagally, Atomic-Scale Mechanisms for Surfactant-Mediated Layer-by-Layer Growth in Homoepitaxy, Phys. Rev. Lett. **72**, 693 (1994).

[24] M. Satta, S. Colonna, R. Flammini, A. Cricenti, and F. Ronci, Silicon Reactivity at the Ag(111) Surface, Phys. Rev. Lett. **115**, 026102 (2015).

[25] S. Xu, Y. Zhao, J. Liao, X. Yang, and H. Xu, The nucleation and growth of borophene on the Ag(111) surface, Nano Res. **9**, 2616 (2016).

[26] G. Kresse and J. Furthmüller, Efficient iterative schemes for *ab initio* total-energy calculations using a plane-wave basis set, Phys. Rev. B **54**, 11169 (1996).

[27] P. E. Blöchl, Projector augmented-wave method, Phys. Rev. B **50**, 17953 (1994).

[28] J. P. Perdew, K. Burke, and M. Ernzerhof, Generalized Gradient Approximation Made Simple, Phys. Rev. Lett. **77**, 3865 (1996).

[29] S. Grimme, J. Antony, S. Ehrlich, and H. Krieg, A consistent and accurate ab initio parametrization of density functional dispersion correction (DFT-D) for the 94 elements H–Pu, J. Chem. Phys. **132**, 154104 (2010).

[30] H. Zi-Pu, D. Ogletree, M. Van Hove, and G. Somorjai, Leed theory for incommensurate overlayers: Application to graphite on Pt(111), Surf. Sci. **180**, 433 (1987).

[31] J. M. Hawkins, J. F. Weaver, and A. Asthagiri, Density functional theory study of the initial oxidation of the Pt(111) surface, Phys. Rev. B **79**, 125434 (2009).

[32] J. Wintterlin and M.-L. Bocquet, Graphene on metal surfaces, Surf. Sci. **603**, 1841 (2009).

[33] P.-Y. Cai, Y.-W. Huang, Y.-C. Huang, M.-C. Cheng, L.-W. Lan, C.-C. Kuo, J.-H. Wang, and M.-F. Luo, Atomic structures of Pt nanoclusters supported on graphene grown on Pt(111), J. Phys. Chem. C **122**, 16132 (2018).

[34] G. Henkelman, B. P. Uberuaga, and H. Jónsson, A climbing image nudged elastic band method for finding saddle points and minimum energy paths, J. Chem. Phys. **113**, 9901 (2000).

[35] J. Gao, Q. Yuan, H. Hu, J. Zhao, and F. Ding, Formation of carbon clusters in the initial stage of chemical vapor deposition graphene growth on Ni(111) surface, J. Phys. Chem. C **115**, 17695 (2011).

[36] D. C. Ford, Y. Xu, and M. Mavrikakis, Atomic and molecular adsorption on Pt(111), Surf. Sci. **587**, 159 (2005).

[37] M. Abon, J. Billy, J. Bertolini, and B. Tardy, Carbon on Pt(111): Characterization and influence on the chemisorptive properties, Surf. Sci. **167**, 1 (1986).

[38] See Supplemental Material at http://link.aps.org/supplemental/10.1103/PhysRevB.108.125425 for the details of the linear relationship between E_f and N_P/N_T, the optimized configurations of C clusters on both the terrace and the lower surface of the

step, along with a comparative analysis between experimental and theoretical works.

[39] Z. Xu and F. Ding, Catalyst geometry dependent single-walled carbon nanotube formation from polyaromatic hydrocarbon molecule: Pt(111) surface versus Pt nanoparticle, Carbon **201**, 483 (2023).

[40] F. Viñes, K. M. Neyman, and A. Görling, Carbon on platinum substrates: From carbidic to graphitic phases on the (111) surface and on nanoparticles, J. Phys. Chem. A **113**, 11963 (2009).

[41] G. Nandamuri, S. Roumimov, and R. Solanki, Chemical vapor deposition of graphene films, Nanotechnology **21**, 145604 (2010).

[42] R. Dronskowski and P. E. Blöchl, Crystal orbital Hamilton populations (COHP): Energy-resolved visualization of chemical bonding in solids based on density-functional calculations, J. Phys. Chem. **97**, 8617 (1993).

[43] P. Merino, L. Rodrigo, A. L. Pinardi, J. Méndez, M. F. López, P. Pou, R. Pérez, and J. A. Martín Gago, Sublattice localized electronic states in atomically resolved graphene-Pt(111) edge-boundaries, ACS Nano **8**, 3590 (2014).

[44] T. A. Land, T. Michely, R. J. Behm, J. C. Hemminger, and G. Comsa, STM investigation of the adsorption and temperature dependent reactions of ethylene on Pt(111), Appl. Phys. A **53**, 414 (1991).

[45] I. Hernández-Rodríguez, J. M. García, J. A. Martín-Gago, P. L. de Andrés, and J. Méndez, Graphene growth on Pt(111) and Au(111) using a MBE carbon solid-source, Diamond Relat. Mater. **57**, 58 (2015).

[46] Z. Xu, R. Zheng, A. Khanaki, Z. Zuo, and J. Liu, Direct growth of graphene on in situ epitaxial hexagonal boron nitride flakes by plasma-assisted molecular beam epitaxy, Appl. Phys. Lett. **107**, 119 (2015).

[47] A. S. Plaut, U. Wurstbauer, S. Wang, A. L. Levy, L. Fernandes dos Santos, L. Wang, L. N. Pfeiffer, K. Watanabe, T. Taniguchi, C. R. Dean, J. Hone, A. Pinczuk, and J. M. Garcia, Exceptionally large migration length of carbon and topographically-facilitated self-limiting molecular beam epitaxial growth of graphene on hexagonal boron nitride, Carbon **114**, 579 (2017).

[48] J. M. Garcia, U. Wurstbauer, A. Levy, L. N. Pfeiffer, A. Pinczuk, A. S. Plaut, L. Wang, C. R. Dean, R. Buizza, A. M. Van Der Zande, J. Hone, K. Watanabe, and T. Taniguchi, Graphene growth on h-BN by molecular beam epitaxy, Solid State Commun. **152**, 975 (2012).